HHS Public Access

Author manuscript

Alzheimers Dement. Author manuscript; available in PMC 2019 February 21.

Published in final edited form as:

Alzheimers Dement. 2019 January ; 15(1): 93–105. doi:10.1016/j.jalz.2018.06.3057.

A nonhuman primate model of early Alzheimer's disease pathologic change: Implications for disease pathogenesis

Caitlin S. Latimer[a], **Carol A. Shively**[b], **C. Dirk Keene**[a], **Matthew J. Jorgensen**[b], **Rachel N. Andrews**[b], **Thomas C. Register**[b], **Thomas J. Montine**[c], **Angela M. Wilson**[a], **Bryan J. Neth**[d], **Akiva Mintz**[e], **Joseph A. Maldjian**[f], **Christopher T. Whitlow**[g], **Jay R. Kaplan**[b], and **Suzanne Craft**[d,*]

[a]Department of Pathology, University of Washington, Seattle, WA, USA

[b]Department of Pathology/Comparative Medicine, Wake Forest School of Medicine, Winston-Salem, NC, USA

[c]Department of Pathology, Stanford University, Stanford, CA, USA

[d]Department of Internal Medicine, Section on Gerontology and Geriatric Medicine, Wake Forest School of Medicine, Winston-Salem, NC, USA

[e]Department of Radiology, Columbia University, New York, NY, USA

[f]Department of Radiology, University of Texas-Southwestern, Dallas, TX, USA

[g]Department of Radiology, Wake Forest School of Medicine, Winston-Salem, NC, USA

Abstract

Introduction: Nonhuman primates may serve as excellent models of sporadic age-associated brain β-amyloid deposition and Alzheimer's disease pathologic changes. We examined whether a vervet nonhuman primate model recapitulated pathologic, physiologic, and behavioral features of early Alzheimer's disease.

Methods: Nine middle-aged (mean = 11.2 years) and nine aged (mean = 21.7 years) female vervet/ African green monkeys underwent cerebrospinal fluid collection, gait speed measurement, and neuroimaging before neuropathologic assessment.

Results: β-amyloid plaques were identified in all aged vervets and paired helical filament tau immunoreactivity was observed in all animals. Cerebrospinal fluid β-amyloid$_{42}$ and gait speed correlated negatively with age and plaque density. Greater plaque and paired helical filament tau burden predicted reduced volumes and CMRg in several brain regions.

Discussion: We observed a coordinated set of relationships among neuropathologic, cerebrospinal fluid, imaging, and behavioral modalities consistent with early Alzheimer's disease. Our results support future use of the vervet model to explore disease mechanisms, biomarkers, and novel therapeutic strategies.

*Corresponding author. Tel.: 1-336-713-8830; Fax: 1-336-713-8826., suzcraft@wakehealth.edu.

Keywords

Alzheimer's disease; Nonhuman primate; Amyloid; Tau; Cerebrospinal fluid (CSF); Model

1. Introduction

Nonhuman primates (NHPs) from old-world species are important translational models of human disease due to their highly conserved genomic sequence, humanoid anatomy, physiology and molecular pathways, and susceptibility to infectious, metabolic, and other diseases [1]. Caribbean vervets *(Chlorocebus aethiops sabaeus*, also known as African green monkeys) imported from Africa to the Caribbean in the 17th century are a nonendangered species that adapts readily to captive social environments and acquires several aging-related metabolic and vascular diseases of relevance to humans. In particular, they may serve as excellent models of age-associated brain β-amyloid (Aβ) deposition due to their phylogenetic proximity and their highly conserved amyloid precursor protein sequence relative to humans. This shared proclivity enables the application of protocols for assessing amyloid burden that are adapted from criteria used for human study, facilitating their use as models of AD-like brain amyloidosis. Aβ accumulation with age is typical in primate brain, as are functional decrements in cognition and mobility with age. Although some studies have suggested that NHPs do not develop prominent neurofibrillary degeneration characteristic of human AD, several reports have documented evidence of abnormal tau phosphorylation in aged NHP brain [2,3] or demonstrated the induction of neurofibrillary tangles after intracerebroventricular administration of oligomeric Aβ [4]. Furthermore, a recent report showed that higher levels of cerebrospinal fluid (CSF) tau-p181 were associated with reduced volume in several brain regions [5].

These and other studies have documented the existence of AD neuropathologic changes in NHP brain and in CSF biomarkers, but the extent of these changes and their relationship to other molecular, structural, and functional characteristics of AD has not been investigated fully. In the present study, we examined age-related AD neuropathologic changes and their relationship to CSF biomarkers, brain structure assessed with magnetic resonance imaging (MRI), cerebral glucose metabolism assessed with ^{18}F-Fluorodeoxyglucose Positron Emission Tomography (^{18}F-FDG PET), and behavior. We observed that, as in humans, Aβ and phospho-tau burden was associated with reduced brain volume and glucose metabolism, as well as with abnormalities of complex integrated behaviors such as gait speed. In addition, the observed Aβ plaque accumulation shares a similar distribution throughout the cerebral cortex as in humans with early AD neuropathologic change. This pattern suggests that aged vervets may be a valuable model to explore Aβ-related mechanisms associated with the earliest stages of AD pathology, as well as to test novel therapeutic strategies.

2. Methods

2.1. Animals

The study animals were nine middle-aged (mean = 11.2, range = 8.2-13.5 years) and nine aged (mean = 21.7, range = 19.5–23.4 years) female vervet/African green monkeys

(*Chlorocebus aethiops sabaeus*). Subjects were born and raised in the multi-generational, pedigreed Vervet Research Colony and housed at Wake Forest School of Medicine, which at the time of the study included 329 descendants of 57 original founders (29 females, 28 males), with matrilines in their second to eighth generation [1]. Colony management practices reflect the natural social composition of vervet monkey groups in the wild. The majority of the colony is housed in 16 enclosures with 1000 sq. ft. of outdoor and 300 sq. ft. of indoor space, each containing one breeding group. All monkeys had free access to standard commercial monkey chow (Purina LabDiet) and water. All procedures involving monkeys were conducted in accordance with state and federal laws, standards of the Department of Health and Human Services, and guidelines established by the Wake Forest Institutional Animal Care and Use Committee.

2.2. Gait speed

The measurement of gait speed has been described in detail previously [6]. Briefly, usual walking speed was quantified via stopwatch as the time it took the monkey to traverse a minimum of 3 feet at a normal pace without provocation [6]. Assessments of usual walking speed were conducted during the day (0700–1600 hours) over the course of a month before necropsy [6]. A minimum of five valid instances were used to calculate mean speed as time per distance traversed.

2.3. Cerebrospinal fluid biomarkers

CSF samples were taken just before necropsy by inserting a 22-gauge needle percutaneously into the cisternal space while the ketamine-sedated animal was maintained in a lateral recumbent position as previously described [7]. Approximately 1–1.5 cm^3 of spinal fluid was obtained and frozen at −70°C until metabolite determinations were made. $A\beta_{1–42}$, total tau, and tau phosphorylated at amino acid 181 (tau-P181) were measured *en block* in first thawed CSF using a Luminex-based INNO-BIA Alzbio3 assay, and $A\beta_{1–40}$ was measured by ELISA according to manufacturer instructions using kits from Fujirebio (Malvern, PA). Coefficients of variation of high and low kit controls for $A\beta_{42}$, total tau, and tau-P181 were all <10%, mean coefficients of variation across all samples were ~ 28% for total tau, and 11%–12% for $A\beta_{1–42}$ and tau-P181. Coefficients of variation for $A\beta_{1–40}$ were <2%.

2.4. Neuroimaging

2.4.1. MRI—MRI imaging was conducted on 15 monkeys from the cohort, who were sedated with ketamine HCl (15 mg/kg body weight, IM) and transported to the imaging center where they were imaged under isoflurane (3% induction, 1.5% maintenance) anesthesia. MRIs were performed on a 3T Siemens Skyra MRI scanner using a circularly polarized, single channel dedicated NHP radiofrequency coil with an internal diameter of 18.4 cm (Litzcage, Doty Scientific, SC). T1-weighted anatomic images were obtained using a 3D volumetric MPRAGE sequence (TR = 2700 msec; TE = 3.39 msec; TI = 880 msec; FA = 8°; 160 slices, voxel dimension = 0.5 x0.5 × 0.5 mm). Structural image analysis was conducted using a NHP imaging pipeline developed at Wake Forest [8,9]. A vervet study-specific template was built using a diffeomorphic shape and intensity averaging technique [10,11]. Skull stripping, segmentation, and label map generation of the study-specific

template was performed using the INIA 19 MRI template and NeuroMap label atlas [12]. A study-specific 6-class tissue probability map and a 6-layer 2-class normalization template were created from the vervet segmentation for use within the SPM VBM8 framework (http://dbm.neuro.uni-jena.de/vbm.html). Fully automated morphologic processing of ver-vet MRI scans was performed using the vervet study-specific tissue probability map and vervet study-specific normalization template [9]. Additional regions of interest were defined using the UNC Primate Brain Atlas label map (http://www.nitrc.org/projects/primate_atlas) warped to the space of the study-specific template. The NHP atlases are fully integrated into PickAtlas software [13] to allow direct region-based hypothesis testing.

2.4.2. FDG PET—Monkeys received PET scans on a separate day from MRI imaging, and identical procedures were used for transport and anesthesia. Scans were performed dynamically on a GE Discovery PET/computed tomography scanner with an isotropic voxel size of 2 mm^3, field-of-view of 25 cm, and an axial field of 18 cm. FDG imaging was conducted using the time frames 12 × 10 sec, 8 × 30 sec, 6 × 4 min, and 3 × 10 min, for a total length of 60 min. An indwelling venous catheter was introduced into a saphenous vein or forearm vein and a second catheter placed in the contralateral saphenous or forearm vein for the injection of 5-10 mCi of tracer. Blood samples were obtained at 3, 8, 16, 24, 35, and 55 min after FDG infusion. Radioactivity in plasma samples was counted in a gamma counter cross-calibrated with the PET scanner. PET images were preprocessed and co-registered to each subject's MR using a cross-modality 3D image fusion tool in PMOD 3.3. Co-registered PET images were corrected for PVE with the modified Müller-Gartner method [14]. Using the PMOD 3.3 pixel-wise kinetic modeling tool, parametric images of CMRg were produced for each animal. CMR quantification requires an arterial input function, determined by tracing regions of interest (ROIs) on the internal carotid arteries with the aid of co-registered MR images as previously validated in humans [15]. The calculated activity within the ROI was corrected using the radioactivity of the plasma samples obtained during PET image acquisition. The lumped constant used for the CMRg calculation was set to 0.80 [16]. CMRg was expressed as mmol/100 g/min using the graphical Patlak model [17].

2.5. Euthanasia and brain retrieval

Animals were euthanized in accordance with guidelines established by the American Veterinary Medical Association, as previously described [18]. Animals were initially anesthetized with ketamine (15–20 mg/kg) and then administered 60–100 mg/kg sodium pentobarbital and maintained at a deep plane of anesthesia. A midline laparotomy was performed, and animals were exsanguinated and the vascular system was flushed with chilled lactated ringer's solution.

Brains were rapidly removed, sectioned in the coronal plane into 7 slices using a rhesus 2-mm slot coronal brain mold (ASI Instruments, Warren, MI), and hemisected. All sections from one side were immediately frozen on dry ice and stored in sealed bags at −80°C for future biochemical studies. All sections from the opposite side of brain were immediately placed into 4% paraformaldehyde for 24 hours, then transferred to 70% alcohol before processing.

2.6. Neuropathology

Paraformaldehyde-fixed tissue sections were processed and embedded in paraffin before sectioning and staining. A microtome was used to cut 4-μm-thick sections from formalin-fixed paraffin-embedded tissue blocks across the anterior-posterior span of each brain, including frontal, parietal, temporal, and occipital lobes, deep nuclei including caudate/putamen and hippocampus, and brainstem and cerebellum. Automated immunohistochemistry was performed on each brain tissue section using standard protocols (Leica BondMax autostainer, Buffalo Grove, IL). Primary antibodies included the following: paired helical filament (PHF)-tau (AT8, Pierce, 1:4200) and Aβ (6E10, Covance, 1:5000). Both antibodies required initial antigen retrieval with incubation in boiling citrate buffer at pH 6.0. Appropriate positive and negative controls were included. To further evaluate for classical AD neuropathologic change, a modified Bielschowsky silver stain was manually performed on 8-μm-thick tissue sections exactly as done for human samples [19].

To compare to age-related pathologic changes in macaques and humans, histopathologic examination was modeled after the National Institute on Aging-Alzheimer's Association Guidelines for the Neuropathologic Assessment of Alzheimer's Disease [20,21], which combines valuations of amyloid plaque distribution (Thal phase, A score), neurofibrillary tangle distribution (Braak stage, B score), and cerebral cortical neuritic plaque density (CERAD score, C score). All neuropathologic assessments were performed blinded to subject identity. The Aβ burden in each brain was assessed across multiple regions in each animal by identifying the area within each region with the highest density and counting the number of plaques in a single 100× field. These counts were then averaged across all the animals that had Aβ plaques, and that average was used to create heat maps of regional Aβ plaque density [22,23]. To further characterize the pattern of AD neuropathologic change, the distribution of Aβ plaques by the method of Thal, et al. [24] using Aβ (6E10) stains, and the distribution of PHF-Tau (AT8) immunoreactive inclusions were assessed in multiple regions from frontal to occipital lobes in each animal. These regions were then mapped onto diagrams of NHP brain. Finally, neuritic plaque burden was assessed for each region per human AD guidelines [25] on a four-point scale (none, sparse, moderate, frequent), and these ratings were summed across all regions for each animal to create a neuritic plaque burden score. An analogous pathologic tau summary score was calculated as the sum of the number of regions for which PHF-tau immunoreactivity was present. The regions reviewed included temporal cortex (superior, middle and inferior temporal gyri), cingulate gyrus, insular cortex, supramarginal cortex, superior frontal gyrus, precentral gyrus, postcentral gyrus, superior parietal lobule, occipital cortex, subiculum, entorhinal cortex, hippocampus, caudate nucleus, putamen, and globus pallidus.

2.7. Protein quantification

Quantification of p-tau variants and Aβ species were determined using a multiplexed Luminex assay. Frozen tissues from temporal and parietal lobe were processed through sequential extraction and centrifugation. Briefly, samples were homogenized by sonicating in 10x volume of reassembly (RAB) buffer (0.1 M 2-(N-morpholino) ethanesulfonic acid), 1 mM ethylene glycol tetraacetic acid, 0.5 mM MgSO4, 0.75 M NaC1, 0.02 M NaF, 1 mM phenylmethylsulfonyl fluoride, 0.1% protease inhibitor), and then centrifuged (Optima TLX

from Beckmann Coulter) at 36,000 rpm for 40 min at 4°C to clarify the homogenate. After supernatants were carefully collected and labeled as RAB extract, the resultant pellets were then re-homogenized in 5M guanidine-HCl or RIPA buffer (50 mM Tris, 150 mM NaCl, 1% Triton x-100, 5 mM ethylenediaminetetraacetic acid, 0.5% sodium deoxycholate, 0.1% lithium dodecyl sulfate, pH 8.0) and centrifuged at 36,000 rpm for 20 minutes at 4°C. Supernatants from the guanidine homogenates were collected and labeled as G extract, and supernatants from the RIPA homogenates were labeled as RIPA extract. The resultant pellets from RIPA homogenates were re-homogenized in 5M guanidine-HCl and centrifuged at 27,000 rpm for 20 minutes at 4°C. All extracts were stored at −80°C until protein quantification was performed with the Luminex Xmap platform (MILLIPLEX kit HNABTMAG-68k). All kit controls were within stated ranges.

Luminex assay was performed according to the Milliplex kit instructions. Briefly, a 96 well plate is washed with assay buffer (Millipore HNABTMAG-68k) and liquid evacuated. Twenty-five micro liters of sample, standard, or control was added to each well. Next 25 µl each of antibody conjugated magnetic beads and biotinylated antibodies were added. Plate was then incubated at room temperature in the dark for 16 hours. Plate was then placed on magnet, liquid evacuated by inversion. The beads remaining in the wells were then washed with assay buffer and the plate magnetized and evacuated. After 3 wash cycles 25 µL Streptavidin Phycoerythrin was added to each well. After 30 minute incubation, the plate was magnetized, evacuated, and washed. Hundred micro liters of buffer was then added to each well, and after 5 minutes of shaking, the plate was read on the instrument. The Bio Rad Bio-Plex software that operates the Luminex was then used to quantify the amount of each protein. A five parameter logistical equation, optimized for the range of responses in the samples, determined the pg/ml concentration of each protein in each well. The concentrations were then normalized to the original weights of the tissue.

2.8. Statistical analyses

Data were analyzed with SAS, version 9.4. Guanidine and RIPA-extracted $A\beta_{42}$ and PHF-tau protein levels in temporal and parietal lobe were analyzed with repeated measures analysis of variance with age category (middle-aged or old) as an independent factor and brain region (temporal or parietal) as the repeated factor. Aβ plaque and PHF-tau burden scores were each subjected to analysis of variance with age category as the independent variable. For MRI volumes and ^{18}F-FDG PET CMRg values, ROIs defined by the UNC atlas were included in a general linear model in which right and left values of a specific region were dependent variables, side (right or left) was a repeated factor, age at necropsy was a covariate, and Aβ plaque density score was the independent variable. Similar analyses were conducted using PHF tau summary score as the independent variable. Spearman rank order correlations were used to examine relationships among neuropathologic, CSF biomarkers, imaging, and behavioral measures.

3. Results

3.1. Neuropathology

The degree of AD neuropathologic change was characterized using a system based on the National Institute on Aging-Alzheimer's Association (NIA-AA) Guidelines for the Neuropathologic Assessment of Alzheimer's Disease [21]; results are summarized in Table 1. Aβ plaques were identified primarily throughout the cortex in all aged vervets and in one middle-aged vervet (Fig. 1A,B), equivalent to a Thal phase 1 [24] or NIA-AA A score of 1. Only one aged vervet had Aβ plaques in the hippocampus (Thal phase 2, NIA-AA A score 1); no Aβ plaques were identified in cerebral deep gray nuclei, brainstem, or cerebellum of any animal. PHF-tau immunoreactivity was observed in all animals; however, it presented only rarely as neurofibrillary change (Fig.1D,E) and never as classic neurofibrillary tangles (Braak 0, NIA-AA B score 0) [26]. Rather, PHF-tau immunoreactive lesions were primarily localized to small cells with granular cytoplasmic immunoreactivity. Aβ plaques were predominantly diffuse; however, of the ten animals with Aβ plaques, eight had neuritic-like plaques identified by Bielschowsky silver stain (Fig. 1F,G) exactly according to established guidelines for human neuropathologic evaluation (CERAD). NIA-AA C score for neuritic plaques for these eight animals ranged from sparse to frequent. By NIA-AA guidelines, the younger vervets, with one exception, were classified as no AD neuropathologic change, while the aged vervets each were classified as low AD neuropathologic change. Other AD-like changes in the older vervets included focal vascular Aβ immunoreactivity that did not appear similar to human cerebral amyloid angiopathy, but rather like endothelial labeling (Fig. 1C).

Semiquantitative assessment of Aβ plaque burden revealed regional variation throughout the cerebral cortex. The temporal cortex, particularly the middle and superior temporal gyri, was most heavily affected. The density pattern is illustrated in a heat map of coronal sections of the vervet brain (Fig. 2). Of the vervets with Aβ plaques in the cerebral cortex, 80% had them in the posterior middle temporal gyrus, 70% in the posterior cingulate gyrus, and 60% in the anterior superior temporal gyrus. Half had Aβ plaques in the anterior middle temporal gyrus, anterior cingulate gyrus, insular cortex, supramarginal cortex, superior frontal cortex, precentral and postcentral gyri, and occipital cortex, while 40% had Aβ plaques in the superior parietal lobule and anterior superior temporal gyrus. Only 30% had plaques in the posterior superior and inferior temporal gyri (Fig. 3A and Table 2) and PHF-tau immunoreactivity (Fig. 3B and Table 3) commonly, but not completely, overlapped. Despite very limited neurofibrillary degeneration, there was substantial PHF-tau immunoreactivity throughout both middle-aged and aged brains, primarily granular and seen in cells with small, round nuclei. Given evidence from a recent study of rhesus macaques that formalin fixation protocols used in human AD neuropathology practice may destroy all but highly fibrillar phosphorylated tau [28], it is possible that the observed immunoreactivity was due in part to nonspecific binding.

An amyloid plaque burden score was constructed by summing the plaque ratings (absent = 0, sparse = 1, moderate = 2, severe = 3) across all brain regions. Older animals showed greater plaque burden than middle-aged animals (mean with (SD) = 0.7 (2.0) for middle

aged vervets, 8.7 (5.8) for old vervets, $P = .0012$). An analogous measure was constructed by summing the number of regions that showed positive PHF-tau immunoreactivity; although values were higher for older than middle-aged animals, this effect did not reach statistical significance (mean with (SD) = 9.9 (5.4) for middle-age animals, 13.4 (6.7) for old animals, $P = .23$).

3.2. Tissue protein quantification

Guanidine-extracted $A\beta_{42}$ or $A\beta_{40}$ levels in temporal and parietal cortex were significantly greater in aged vervets compared with middle-aged animals (ps < 0.05; Fig. 4A). No age-related or regional difference was observed for RIPA-extracted $A\beta_{42}$ or $A\beta_{40}$.

Higher levels of guanidine-extracted PHF-tau were observed in parietal compared to temporal cortex for both younger and older groups ($P < .001$; Fig. 4B). In contrast, RIPA-extracted PHF-tau was higher in temporal cortex for older animals, whereas no age difference was observed for parietal cortex (age by region $P < .04$). To explore the possibility that immunohistochemical measurements of PHF tau were distorted due to the use of formalin-fixed tissue as prescribed in human protocols, we correlated RIPA- and guanidine-extracted PHF tau measured in frozen tissue with the tau summary score derived from the immunohistochemical analyses. RIPA-extracted PHF tau in temporal cortex was positively correlated with the tau summary score (Rho = 0.48, $P < .05$). No associations were observed between parietal measures or guanidine-extracted levels.

RIPA-extracted total tau was higher in temporal than parietal cortex for both age groups ($P < .05$). As expected, total tau was not detected in the guanidine-extracted fraction in parietal regions, and only small amounts in temporal cortex that did not differ by age.

3.3. CSF biomarkers

As in humans, CSF $A\beta_{42}$ and $A\beta_{40}$ levels correlated negatively with age (Rhos = −0.54, $P < .02$ and −0.64, $P < .004$) and Aβ plaque density (Rhos = −0.47, $P < .05$ and −0.42, P < .08). CSF $A\beta_{42}$ was inversely related to guanidine-extracted $A\beta_{42}$ in temporal cortex, with a similar trend for parietal cortex (Rhos = −0.47, $P < .05$ and −0.42, P < .09). CSF $A\beta_{40}$ was negatively associated with guanidine-extracted $A\beta_{42}$ in parietal cortex (Rho = 0.48, $P < .05$). No associations were observed between age, $A\beta_{42}$, or $A\beta_{40}$ and CSF tau or tau-P181.

3.4. Gait speed

Gait speed reflects integration of complex cognitive and motor processes, and slower gait speed is an early behavioral indicator of risk for cognitive decline, AD, and other dementias [29]. Slower gait speed was associated with increased age (Rho = −0.60, $P = .05$), lower CSF $A\beta_{42}$ levels (Rho = 0.70, $P < .02$) and greater concentrations of guanidine-extracted $A\beta_{42}$ in temporal lobe with a similar trend in parietal regions (Rhos = −0.47, $P < .05$ and −0.42, $P < .09$). A trend was also noted for greater PHF-tau burden and slower gait speed (Rho = −0.57, $P = .07$).

3.5. Brain imaging

The relationships between Aβ plaque burden scores and MRIROI values were examined for animals with Aβ plaques. Aβ plaque burden interacted with age such that older animals with greater Aβ plaque burden had reduced volumes in several brain regions (bilateral frontal, and left prefrontal and putamen (ps < 0.05), with similar trends observed for bilateral parietal, left insula and cingulate, and right caudate (all ps < 0.10). Greater PHF-tau burden was associated with reduced volume bilaterally in insula and cerebellum, as well as in left temporal lobe (ps < 0.05) with similar trends noted in bilateral cingulate and right temporal lobe (ps < 0.10). Smaller MRI volumes in right prefrontal, left inferior, and left posterior temporal cortex were associated with higher levels of CSF tau-P181 (Rhos = −0.62, −0.69, and −0.63; ps < 0.02, 0.01, and 0.02; Fig. 5A–C), with similar trends for right insula and left frontal (ps < 0.08). No association with MRI volumes was observed for CSF $A\beta_{42}$ or $A\beta_{40}$.

For ^{18}F-FDG PET measures, Aβ plaque density was associated with reduced CMRg in multiple ROIs, with significant ($P < .05$) reductions in bilateral hippocampus, parietal, occipital and cerebellar ROIs, as well as in left temporal lobe. Similar trends ($P < .10$) were observed in bilateral frontal, prefrontal, cingulate, and amygdala, as well as in right temporal and putamen. Age adjustment did not affect the pattern of results. No significant effects were observed for PHF-tau burden, or the interaction between age and PHF-tau burden.

For biochemical analyses, higher guanidine-extracted tau-P181 in parietal cortex was associated with reduced CMRg in all brain regions with or without age adjustment (all ps < 0.05). No relationships were observed between CMRg in any ROI and guanidine extracted tau-P181 in temporal cortex; levels of RIPA-extracted tau-P181 in parietal or temporal cortex were also unrelated to CMRg. Interestingly, the reverse regional pattern was observed for guanidine-extracted $A\beta_{42}$; higher levels were related to reduced CMRg in temporal cortex for nearly all regions studied (ps < 0.05 for bilateral parietal, temporal visual and limbic, occipital, cingulate, hippocampus, amygdala, cerebellum, right prefrontal, frontal, and insula; ps < 0.10 for left prefrontal cortex, amygdala and insula, right caudate nucleus, and putamen), whereas no relationships were observed for parietal cortex. Total tau was unrelated to CMRg in any region.

For CSF biomarkers, lower $A\beta_{42}$ was associated with lower CMRg in numerous regions including left hippocampus, caudate nucleus, putamen, cerebellum, occipital, and pons ROIs, and right cingulate, insula, and occipital ROIs (all ps < 0.05; Fig. 6A,B). Similar trends were noted for left temporal, frontal, and prefrontal ROIs and right hippocampus, amygdala, and putamen. No relationship was observed between CMRg and $A\beta_{40}$ or tau-p181.

4. Discussion

There is a great need for AD animal models that more closely replicate complex human disease to augment elegant mechanistic work accomplished in rodent models. To address this need, we have conducted a comprehensive pre-mortem and postmortem examination of a cohort of middle-aged and aged NHPs performed in a manner comparable to the current guidelines for human neuropathologic evaluation of AD. The hallmark pathologic features

of AD have been observed in the brains of great apes, including chimpanzees and orangutans, as well as Old World Monkeys, such as vervets and macaques [30–35]. The great apes have the closest phylogenic relationship to humans; however, studies involving these animals are scarce and tissue resources are limited. Vervets, conversely, are non-endangered Old World Monkeys that adapt well to captivity and are increasingly being used as models due to their proclivity to develop diseases relevant to humans in the course of aging without genetic manipulation. The present study leveraged a series of planned necropsies in a cohort of middle-aged and aged female vervets and performed prospective evaluations similar to research cohorts of human participants for the study of AD, including fasting blood and CSF collection, assessment of gait speed, and neuroimaging. The purpose of the study was to determine whether this NHP model recapitulated pathologic, physiologic, and behavioral features of early AD.

4.1. Aged vervets show human-like amyloid neuropathologic change

In this study, the neuropathologic evaluation followed recent guidelines for the assessment of AD in humans [21]. At the time of death, the collection, storage, and analysis of the brain tissue was aligned with human protocols, and NIA-AA guidelines for sampling and histopathological assessment of human AD were followed. These guidelines are particularly useful in this model because the NIA-AA criteria, unlike their predecessors, are focused exclusively on neuropathologic changes without consideration of clinical changes, cognitive symptoms or age. Histologically, amyloid plaques observed in the vervets, which develop spontaneously with advancing age, were remarkably similar to those seen in human AD. Detailed studies on the distribution and density of amyloid plaques in humans have shown that the temporal lobe is involved often and early, particularly the medial temporal lobe [36]. Here, assessing amyloid plaque distribution according to Thal et al. in humans [24], we show that vervets also most often have amyloid plaques in the temporal lobe, although more frequently localized to middle and superior temporal gyri with the inferior and medial portions less involved. Aβ deposition was also frequently observed in older vervets in the posterior cingulate gyrus, a region that is affected early in AD [37]. The distribution of Aβ deposition in human cortex described by Thal et al. [24] showed that Aβ plaques in nondemented individuals were typically confined to the cortex and allocortex, occasionally extending to the striatum. It is often postulated that the presence of such changes in the absence of dementia may represent early (preclinical) AD in which the clinical manifestations of the pathology had not yet become apparent [21]. Thus vervets may be a relevant model of very early AD because Aβ deposits develop naturally as a function of age and in a similar distribution as in humans, before the occurrence of widespread neuron loss and dysfunction characteristic of end-stage disease.

The results pertaining to tau were more complex. A summary index of pTau immunohistochemistry was related to levels of RIPA-extracted PHF tau in frozen tissue from temporal cortex, as well as to reduced MRI volumes in temporal lobe. However, when ABC scores were assigned only “not” and “low” AD neuropathologic change were identified, due to the absence of true neurofibrillary degeneration identified using pTau (AT8) immunohistochemistry and Bielschowsky silver histochemical stain. The sparsity of neurofibrillary tangles is consistent with previous studies in vervets [32], as well as in other

NHP species [38]. Here, although few true tangles were identified, we did note positive immunoreactivity for PHF-tau in both middle aged and old animals, but the neuroanatomical and cell type distribution and cytolocalization identified in this study overlap, but do not mirror, those in humans. As with human AD, hyperphosphorylated tau immunohistochemical staining was most frequently observed in entorhinal cortex, but other regions of the medial temporal cortex that contribute to the earlier Braak stages, such as hippocampus and subiculum, were less often involved. Furthermore, PHF-tau was unexpectedly noted in the occipital cortex while other more commonly affected regions in human disease were spared. Finally, PHF-tau immunoreactivity was primarily limited to small cells, while in humans, PHF-tau is identified in larger, projection neurons as well as smaller cells and tends to be distributed throughout the soma in a granular (pretangle) and then fibrillar (tangle) pattern with extension into neurites (so-called “neuritic tau”).

Potential explanations for these differences must be considered. In a study by Paspalas et al. [28] evaluating AD-like pathologic changes in rhesus macaques, they reported Braak-like distribution and cytopathologic features of PHF-tau (AT8) immunostaining highlighting tau pathology that was lost after formaldehyde fixation. Given that the goal of the present study was to compare AD-like pathology in aging vervets using protocols aligned with human neuropathological protocols, we deliberately used antibodies and formaldehyde fixation protocols aligned with those used in assessment of human AD neuropathologic change. We recognize the likelihood that early species of pTau may be undetectable using these protocols and future studies of aging vervets that undergo perfusion but not formaldehyde fixation are needed to further explore the patterns of pTau pathology in this model. Another explanation may relate to the complexity of the vervet versus rhesus macaque brain as compared with humans; increased connectivity particularly with respect to cortical-cortical connections in rhesus macaques may be permissive for more advanced pTau, and therefore fibrillar tau, pathology. This possibility is supported by Paspalas et al., in which eleven rhesus macaques demonstrated a similar pattern of pathologic tau as vervets and humans, beginning with phosphorylated nonfibrillar tau in layer II of the entorhinal cortex in young adulthood, and progressing to Braak stage III in older animals. Mature NFTs were observed in the oldest animal. Finally, pTau distribution patterns across species may vary as a result of functional differences. Future studies across different animal species to corroborate functional and structural mapping and registration with AD pathologic change are needed, and may provide important clues as to the processes that promote tangle formation and propagation in humans. For example, although increased tau phosphorylation throughout the brain has been reported in a vervet model of streptozotocin-induced type 1 diabetes [39], it will be important for future investigations to develop and test various hypotheses about specific mechanistic processes that promote tangle formation and propagation in humans. In addition, studies should be powered to explore possible sex-differences in these processes. The results presented here, along with future studies, will provide a strong basis for the value of NHP models of early AD.

4.2. CSF and neuroimaging biomarkers are associated with neuropathological indices

As in humans, CSF $A\beta_{42}$ levels correlated negatively with Aβ plaque density [40–43]. These results demonstrate the relative ease with which biomarker protocols that closely follow

those used in humans for the pre-mortem evaluation of neurodegenerative disease can be implemented in a NHP model as well as the relevance of the changes identified in these animals to humans. Our results are partially consistent with a recent report of AD CSF biomarkers in a cohort of 329 vervets ranging in age from 1 to 27 years, which included CSF samples taken at an earlier age from 12 of the animals in the present study, although inconsistencies were noted as well. In both studies, CSF Aβ, tau and tau-p181 were measured with identical methods [5], and CSF $A\beta_{40}$ was negatively correlated with age. However, unlike the present results, CSF $A\beta_{42}$ was not correlated with age for the larger cohort study. One possible explanation is that CSF $A\beta_{42}$ does not decline linearly across the entire lifespan, but only declines after middle age in conjunction with age-related compromise of clearance and subsequent sequestration of Aβ into plaques. In other models such as canines, high CSF $A\beta_{42}$ is associated with memory impairment in young and middle aged animals, whereas low levels are associated with impairment in older animals [44].

Neuroimaging markers also showed typical relationships with neuropathological indices. Aβ plaque burden was associated with reduced volume in several AD-related regions, such as frontal cortex, parietal cortex, insula and cingulate, similar to human studies demonstrating Aβ-related atrophy patterns in heteromodal cortical areas in preclinical adults [45]. Greater Aβ pathology, as indicated by lowered CSF $A\beta_{42}$ and elevated plaque burden, was also associated with reduced cerebral glucose utilization in multiple brain regions, similar to reports in humans [40–43]. PHF-tau burden was also related to reduced volumes in these regions, and in temporal cortex. Relationships between tau assessed with ^{18}F AV-1451 PET imaging and temporal cortical thickness assessed with MRI have been noted in older adults [46]. Furthermore, although CSF and immunohistochemical measures of tau-P181 were unrelated to cerebral glucose utilization, increased biochemical measures of fibrillar (guanidine-extracted) tau-P181 in parietal cortex were associated with reduced glucose metabolism in all brain regions. This result is consistent with human studies in which greater deposition of tau aggregates measured via ^{18}F AV-1451 correlated with reduced cerebral glucose metabolism measured with ^{18}F FDG [47]. It is notable, however, that even in the absence of pervasive neurofibrillary tangles which are targeted by ^{18}F AV-1451, tau-P181 measured in brain tissue was associated with neuroimaging markers of atrophy and hypometabolism. These findings suggest that hyperphosphorylated tau can negatively impact the brain before or independent of neurofibrillary tangle formation.

4.3. AD pathologic change predicts behavior

In the present study, we measured gait speed in freely moving animals as a behavioral index. Gait speed is a complex index of higher cognitive and motoric integration, and can be assessed in NHPs living in naturalistic social groups [48]. Studies in humans demonstrate a relationship between slowing of gait speed and declining cognition in both normal aging and AD [49,50]. In recent work, gait speed in cognitively normal adults was related to Aβ accumulation in multiple brain regions as assessed with C^{11} PiB PET, even after adjusting for age, neurodegeneration and comorbidities such as hypertension [51]. Other studies have also reported a relationship between Aβ accumulation and gait speed in adults with MCI and AD [49], and associations with the severity of AD neuropathologic change seen at autopsy [52]. In our NHP cohort, slower gait speed was associated with lower CSF $A\beta_{42}$ levels and

greater density of Aβ plaques, with a similar trend noted for tau burden, even after controlling for age. This pattern supports the notion that gait speed can be used as a behavioral marker of AD neuropathologic change in vervets.

4.4. Limitations and future directions

Research with NHPs focused on AD is at an early stage, and thus offers the opportunity to "synthesize early or pilot data into new testable conceptual models" as recommended by a recent editorial by Khachaturian et al. [53]. Vervets and other NHP species, while promising models, have several characteristics that should be addressed in future work to fully ascertain their applicability to human disease: (1) As discussed, although fibrillar tau can be detected with biochemical assays, vervets do not typically exhibit widespread neurofibrillary tangles or prominent humanoid tauopathy. Whether this difference is due to species-specific differences in the tau protein, or in conditions that promote tauopathy has not been determined, and would be a fruitful area of study, not only for the validation of this model, but to discover factors associated with resistance to tangle formation and propagation that could be translated into human therapeutics; (2) Although vervets exhibit reduced brain volume in association with amyloid deposition, they do not exhibit widespread neurodegeneration. This protection may be associated with the aforementioned lack of tauopathy, given that in humans pronounced neurodegeneration is typically associated with later Braak stages. Studies aimed at elucidating this association will also offer insight into re-silience that may inspire new therapeutic approaches; and (3) although vervets and other NHPs show changes in cognition and behavior associated with amyloid deposition, they do not exhibit frank dementia. Again, in humans, significant impairments in cognition and function appear to be synchronized with the acceleration of tangles detected with PET, and thus differences in tau regulation in vervets and other NHPs may explain this protection. Taken together, these limitations reinforce the notion that vervets are best considered a model of early amyloid pathology and corresponding behavioral and biomarker changes, which makes them valuable for the study of early stages of AD. Additionally, their resistance to the development of widespread tau pathology may support their value for the study of mechanisms that protect against triggering of tau pathology by amyloid, or for other resilience-related factors.

To fully investigate the value of the vervet model, several methodologic limitations must also be addressed: (1) more extensive longitudinal characterization is needed to determine the trajectory of decline in cognition, behavior, and AD biomarkers, and identifying specific interrelationships among these parameters that differentiate AD pathology from normal aging; and (2) Small numbers of animals in studies may produce underpowered or spurious results. The use of relatively small sample sizes is typical in NHP studies given ethical considerations and expense. This limitation can be offset in part by intensive phenotyping of study animals, including brain immunohistochemistry and biochemical analyses, CSF analyses, multi-modal imaging and behavioral characterization. Alignment of protocols across NHP programs may enable pooling of data and tissue to increase numbers. Furthermore, careful control of environmental factors such as diet and social milieu, and standardized monitoring of physiologic parameters over timeframes which capture long exposures in "human years", may make relationships among environmental, biologic and

genetic mechanisms easier to detect with smaller numbers; and 3) Strict application of human tissue preparation protocols may distort some aspects of NHP pathology such as immunohistochemical measures of PHF tau. Development of protocols adapted to species-specific differences in brain chemistry may be needed to fully characterize NHP models.

Although previous work has documented AD neuropathologic change in vervet and other NHP models, our study is the first to apply human NIA-AA guidelines to evaluate neuropathologic changes, and then demonstrate the relationship between these changes and human AD-like characteristics of lower CSF $A\beta_{42}$, reduced brain volume and metabolism, and behavior in the same NHPs that have been neuropathologically characterized. In the face of predictions of escalating AD prevalence, a lack of effective treatment options, and animal models that do not adequately capture the complexity of sporadic late-onset AD, there is a growing interest in NHPs as a potential translational model of this devastating disease. For example, NHPs may serve as important intermediary models for therapeutic agents that appear promising in rodents, before engaging in expensive or risky trials in human participants. NHP models may also be useful for discovery of complex disease mechanisms that more closely approximate human disease.

As a species, vervets adapt well to captivity and are increasingly being used to model various human diseases and to test important questions that may enhance the development of effective prevention or treatment strategies. Like humans, aged vervets experience a decline in functions such as gait speed, develop various co-morbid conditions known to increase AD risk such as obesity, diabetes, hypertension, and cardiovascular disease, and develop age-related AD-like amyloid changes without genetic manipulation. We observed a coordinated set of relationships among neuropathologic, CSF, imaging, and behavioral modalities that are consistent with early AD, a crucial time-point in which to intervene and prevent disease progression. Our results provide strong support for future studies using this model to explore disease mechanisms, identify new biomarkers, and test novel therapeutic strategies.

Acknowledgments

This work was supported by the Wake Forest Alzheimer's Disease Core Center (P30- AG049638), the Vervet Research Colony (P40-OD010965), and the Roena B. Kulynych Center for Memory and Cognition Research. The authors thank Tara Chavanne, Margaret Long, Edison Floyd, Jean Gardin, Dianna Swaim, Dewayne Cairnes, Joshua Long, Beth Uber-seder, Ben Wagner, and Dr. Hannah Atkins for technical assistance. They also would like to acknowledge the contributions of the Wake Forest Clinical and Translational Science Institute.

References

[1]. Jasinska AJ, et al. Systems biology of the vervet monkey. Ilar J 2013; 54:122–43. [PubMed: 24174437]

[2]. Carlyle BC, et al. cAMP-PKA phosphorylation of tau confers risk for degeneration in aging association cortex. Proc Natl Acad Sci U S A 2014;111:5036–41. [PubMed: 24707050]

[3]. Darusman HS, et al. Amyloid Beta1-42 and the Phoshorylated Tau Threonine 231 in Brains of Aged Cynomolgus Monkeys (Macaca fascicularis). Front Aging Neurosci 2014;6:313. [PubMed: 25426069]

[4]. Forny-Germano L, et al. Alzheimer's disease-like pathology induced by amyloid-beta oligomers in nonhuman primates. J Neurosci 2014; 34:13629–43. [PubMed: 25297091]

[5]. Chen JA, et al. Neurodegenerative disease biomarkers Aβ1–40, Aβ1–42, tau, and p-tau181 in the vervet monkey cerebrospinal fluid: Relation to normal aging, genetic influences, and cerebral amyloid angiopathy. Brain Behav 2018;8:e00903. [PubMed: 29484263]

[6]. Shively CA, et al. Aging and physical mobility in group-housed Old World monkeys. Age (Dordr) 2012;34:1123–31. [PubMed: 22203457]

[7]. Shively CA, et al. Sertraline effects on cerebrospinal fluid monoamines and species-typical socioemotional behavior of female cynomolgus monkeys. Psychopharmacology (Berl) 2014;231:1409–16. [PubMed: 24193371]

[8]. Maldjian JA, et al. Multi-Atlas library for eliminating normalization failures in non-Human primates. Neuroinformatics 2016;14:183–90. [PubMed: 26643442]

[9]. Maldjian JA, et al. Vervet MRI atlas and label map for fully automated morphometric analyses. Neuroinformatics 2014;12:543–50. [PubMed: 24850577]

[10]. Avants B, Gee JC. Geodesic estimation for large deformation anatomical shape averaging and interpolation. Neuroimage 2004; 23:S139–50. [PubMed: 15501083]

[11]. Avants BB, et al. Symmetric diffeomorphic image registration with cross-correlation: evaluating automated labeling of elderly and neurodegenerative brain. Med Image Anal 2008;12:26–41. [PubMed: 17659998]

[12]. Rohlfing T, et al. The INIA19 Template and NeuroMaps Atlas for Primate Brain Image Parcellation and Spatial Normalization. Front Neuroinform 2012;6:27. [PubMed: 23230398]

[13]. Maldjian JA, et al. An automated method for neuroanatomic and cytoarchitectonic atlas-based interrogation of fMRI data sets. Neuroimage 2003;19:1233–9. [PubMed: 12880848]

[14]. Quarantelli M, et al. Integrated software for the analysis of brain PET/ SPECT studies with partial-volume-effect correction. J Nucl Med 2004;45:192–201. [PubMed: 14960635]

[15]. Zhou S, et al. A method of generating image-derived input function in a quantitative (1)(8)F-FDG PET study based on the shape of the input function curve. Nucl Med Commun 2011;32:1121–7. [PubMed: 21946619]

[16]. Graham MM, et al. The FDG lumped constant in normal human brain. J Nucl Med 2002;43:1157–66. [PubMed: 12215553]

[17]. Patlak CS, Blasberg RG, Fenstermacher JD. Graphical evaluation of blood-to-brain transfer constants from multiple-time uptake data. J Cereb Blood Flow Metab 1983;3:1–7. [PubMed: 6822610]

[18]. Shively CA, et al. Depressive behavior and coronary artery atherogenesis in adult female cynomolgus monkeys. Psychosom Med 2008; 70:637–45. [PubMed: 18596246]

[19]. Yamamoto T, Hirano A. A comparative study of modified Bielschow- sky, Bodian and thioflavin S stains on Alzheimer's neurofibrillary tangles. Neuropathol Appl Neurobiol 1986;12:3–9. [PubMed: 2422580]

[20]. Hyman BT, et al. National Institute on Aging-Alzheimer's Association guidelines for the neuropathologic assessment of Alzheimer's disease. Alzheimer's Dement 2012;8:1–13. [PubMed: 22265587]

[21]. Montine TJ, et al. National Institute on Aging-Alzheimer's Association guidelines for the neuropathologic assessment of Alzheimer's disease: a practical approach. Acta Neuropathol 2012;123:1–11. [PubMed: 22101365]

[22]. Woods RP, et al. A web-based brain atlas of the vervet monkey, Chlorocebus aethiops. Neuroimage 2011;54:1872–80. [PubMed: 20923706]

[23]. Rohlfing T, et al. The INIA19 template and neuroMaps atlas for primate brain image parcellation and spatial normalization. Front Neuroinformatics 2012;6(27).

[24]. Thal DR, et al. Phases of A beta-deposition in the human brain and its relevance for the development of AD. Neurology 2002;58:1791–800. [PubMed: 12084879]

[25]. Mirra SS, et al. The Consortium to Establish a Registry for Alzheimer's Disease (CERAD). Part II. Standardization of the neuropathologic assessment of Alzheimer's disease. Neurology 1991; 41:479–86. [PubMed: 2011243]

[26]. Braak H, Braak E. Staging of alzheimer's disease-related neurofibrillary changes. Neurobiol Aging 1995;16:271–8. [PubMed: 7566337]

[27]. Thal DR, et al. Alzheimer-related tau-pathology in the perforant path target zone and in the hippocampal stratum oriens and radiatum correlates with onset and degree of dementia. Exp Neurol 2000;163:98–110. [PubMed: 10785448]

[28]. Paspalas CD, et al. The aged rhesus macaque manifests Braak stage III/IV Alzheimer' s-like pathology. Alzheimers Dement 2018; 14:680–91. [PubMed: 29241829]

[29]. Mielke MM, et al. Assessing the temporal relationship between cognition and gait: slow gait predicts cognitive decline in the Mayo Clinic Study of Aging. J Gerontol A Biol Sci Med Sci 2013;68:929–37. [PubMed: 23250002]

[30]. Edler MK, et al. Aged chimpanzees exhibit pathologic hallmarks of Alzheimer's disease. Neurobiol Aging 2017;59:107–20. [PubMed: 28888720]

[31]. Poduri A, et al. Apolipoprotein E4 and beta amyloid in senile plaques and cerebral blood vessels of aged rhesus monkeys. Am J Pathol 1994; 144:1183–7. [PubMed: 8203459]

[32]. Kalinin S, et al. Development of amyloid burden in African Green monkeys. Neurobiol Aging 2013;34:2361–9. [PubMed: 23601810]

[33]. Lemere CA, et al. Alzheimer's disease abeta vaccine reduces central nervous system abeta levels in a non-human primate, the Caribbean vervet. Am J Pathol 2004;165:283–97. [PubMed: 15215183]

[34]. Selkoe DJ, et al. Conservation of brain amyloid proteins in aged mammals and humans with Alzheimer's disease. Science 1987;235:873–7. [PubMed: 3544219]

[35]. Cork LC, et al. Development of senile plaques. Relationships of neuronal abnormalities and amyloid deposits. Am J Pathol 1990; 137:1383–92. [PubMed: 1701963]

[36]. Thal DR, et al. Sequence of Abeta-protein deposition in the human medial temporal lobe. J Neuropathol Exp Neurol 2000;59:733–48. [PubMed: 10952063]

[37]. Herholz K, et al. Discrimination between Alzheimer dementia and controls by automated analysis of multicenter FDG PET. Neuroimage 2002;17:302–16. [PubMed: 12482085]

[38]. Walker LC, Jucker M. The Exceptional Vulnerability of Humans to Alzheimer's Disease. Trends Mol Med 2017;23:534–45. [PubMed: 28483344]

[39]. Morales-Corraliza J, et al. Brain-Wide Insulin Resistance, Tau Phosphorylation Changes, and Hippocampal Neprilysin and Amyloidbeta Alterations in a Monkey Model of Type 1 Diabetes. J Neurosci 2016;36:4248–58. [PubMed: 27076423]

[40]. Engelborghs S, et al. Diagnostic performance of a CSF-biomarker panel in autopsy-confirmed dementia. Neurobiol Aging 2008; 29:1143–59. [PubMed: 17428581]

[41]. Erten-Lyons D, et al. Neuropathological basis of age-associated brain atrophy. JAMA Neurol 2013;70:616–22. [PubMed: 23552688]

[42]. Kotrotsou A, et al. Neuropathologic correlates of regional brain volumes in a community cohort of older adults. Neurobiol Aging 2015; 36:2798–805. [PubMed: 26195068]

[43]. Toledo JB, et al. Clinical and multimodal biomarker correlates of ADNI neuropathological findings. Acta Neuropathol Commun 2013; 1:65. [PubMed: 24252435]

[44]. Borghys H, et al. Young to middle-Aged dogs with high amyloid-beta levels in cerebrospinal fluid are impaired on learning in standard cognition tests. J Alzheimers Dis 2017;56:763–74. [PubMed: 28035921]

[45]. Whitwell JL, et al. Does amyloid deposition produce a specific atrophic signature in cognitively normal subjects? Neuroimage Clin 2013;2:249–57. [PubMed: 24179779]

[46]. Maass A, et al. Entorhinal tau pathology, episodic memory decline, and neurodegeneration in aging. J Neurosci 2018;38:530–43. [PubMed: 29192126]

[47]. Ossenkoppele R, et al. Tau PET patterns mirror clinical and neuroanatomical variability in Alzheimer's disease. Brain 2016;139:1551–67. [PubMed: 26962052]

[48]. Morris R, et al. Gait and cognition: Mapping the global and discrete relationships in ageing and neurodegenerative disease. Neurosci Biobehav Rev 2016;64:326–45. [PubMed: 26915926]

[49]. Nadkarni NK, et al. Association of brain amyloid-beta with slow gait in elderly individuals without dementia: Influence of cognition and apolipoprotein E epsilon4 genotype. JAMA Neurol 2017;74:82–90. [PubMed: 27842173]

[50]. Taylor ME, et al. Slow gait speed is associated with executive function decline in older people with mild to moderate dementia: A one year longitudinal study. Arch Gerontol Geriatr 2017;73:148–53. [PubMed: 28818760]

[51]. Wennberg AMV, et al. Cerebral amyloid deposition is associated with gait parameters in the mayo clinic study of aging. J Am Geriatr Soc 2017;65:792–9. [PubMed: 27869301]

[52]. Buchman AS, et al. Physical frailty in older persons is associated with Alzheimer disease pathology. Neurology 2008;71:499–504. [PubMed: 18695161]

[53]. Khachaturian AS, et al. New thinking about thinking, part two. Theoretical articles for Alzheimer's & Dementia. Alzheimers Dement 2018;14:703–6. [PubMed: 29842864]

RESEARCH IN CONTEXT

1. Systematic review: Using PubMed, the authors identified articles concerning nonhuman primate models of sporadic Alzheimer's pathology. Studies have documented the existence of at least some Alzheimer's disease (AD) neuropathologic changes in the nonhuman primate brain and in CSF biomarkers, but the extent of these changes and their relationship to other molecular, structural, and functional characteristics of AD has not been investigated fully.
2. Interpretation: Our results highlighted important relationships between neuropathologic, CSF, imaging, and behavioral modalities that are consistent with early AD. Thus, our sporadic nonhuman primate model may serve a role in helping to better understand AD.
3. Future directions: There is a great need for AD animal models that more closely replicate complex human disease to augment elegant mechanistic work accomplished in rodent models. Future studies may use this and similar models of sporadic early AD to explore disease mechanisms, identify new biomarkers, and test novel therapeutic strategies.

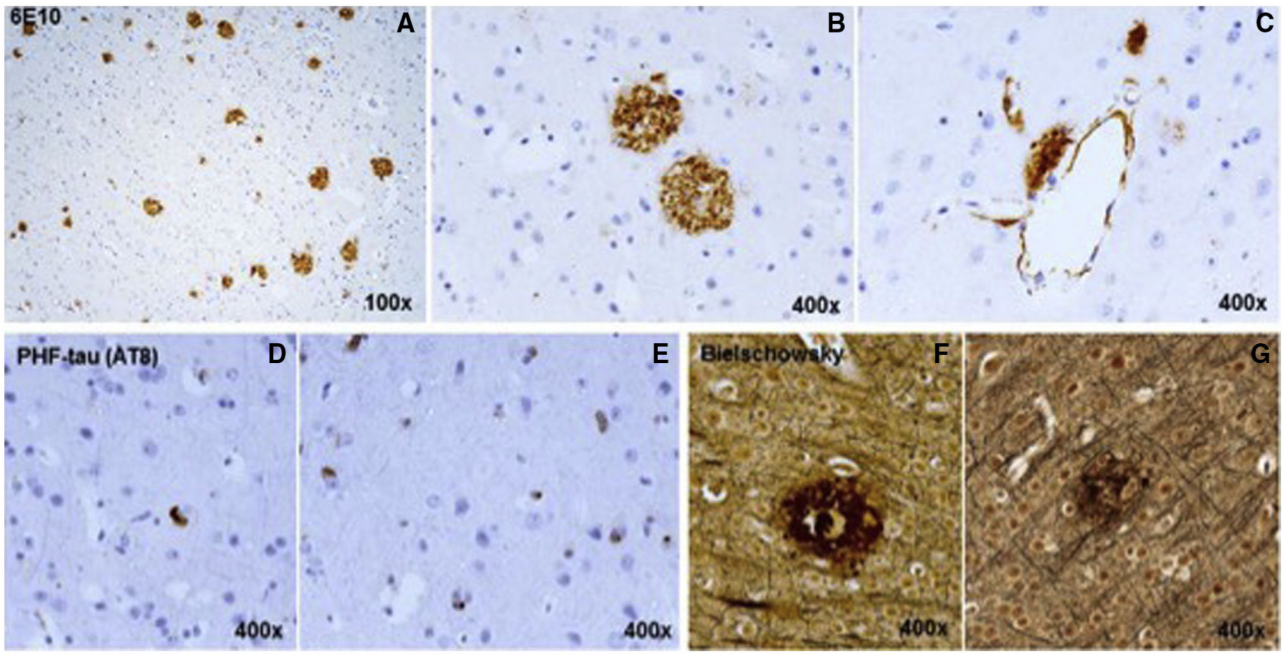

Fig. 1.

(A), (B) Aβ plaques were histologically similar to those seen in human AD. (C) Focal vascular wall Aβ was also noted. (D), (E) granular cytoplasmic PHF-tau aggregates were present, but neurofibrillary tangles were rare. (F), (G) neuritic plaques were confirmed with Bielschowsky stain. Abbreviations: Aβ, β-amyloid; AD, Alzheimer's disease; PHF, paired helical filament.

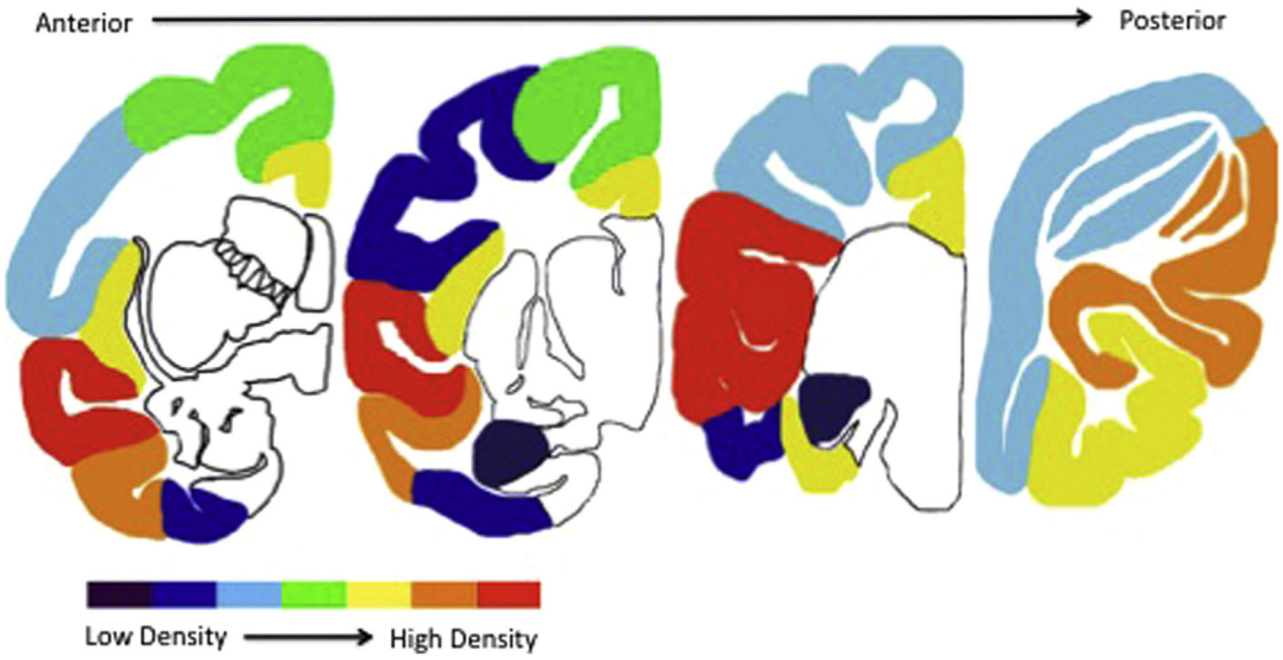

Fig. 2.

The density of Aβ pathology is illustrated on a heat map. On average, Aβ plaque density is highest in the lateral temporal lobe and lowest in the medial temporal lobe regions. Aβ pathology was not identified in deep cerebral nuclei, brainstem, or cerebellum.

Abbreviation: Aβ, β-amyloid.

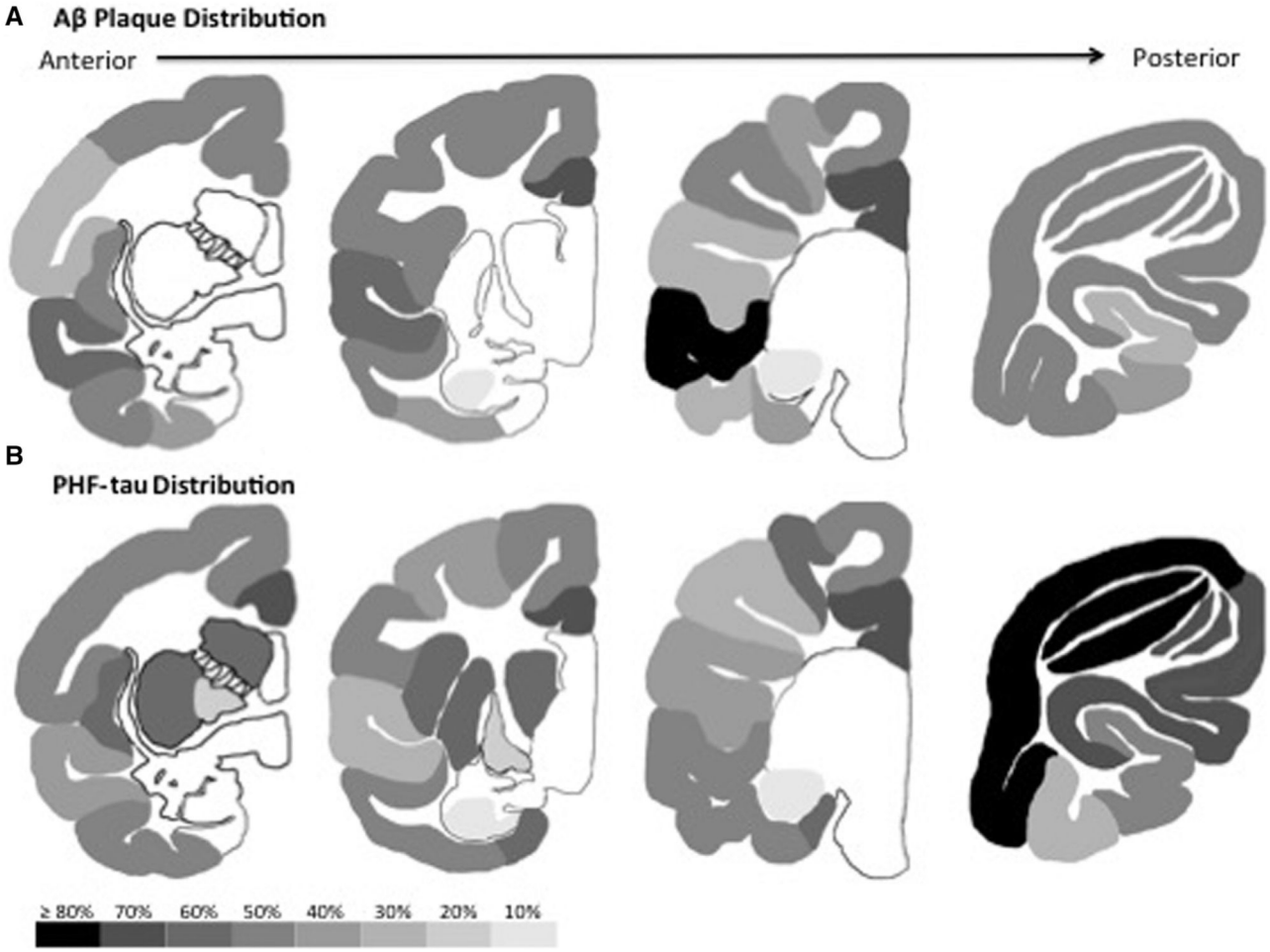

Fig. 3.

The frequency with which AD neuropathologic change is identified in various brain regions is illustrated by increasing shades of gray such that the more frequently affected areas are darker. (A) Aβ plaques are distributed throughout the cerebral cortex and are most often found in the posterior middle temporal gyrus followed by the posterior cingulate gyrus. (B) PHF-tau immunoreactivity is distributed throughout the cortex and the deep gray nuclei, including caudate nucleus, putamen, and globus pallidus. Abbreviations: Aβ, β-amyloid; AD, Alzheimer's disease; PHF, paired helical filament.

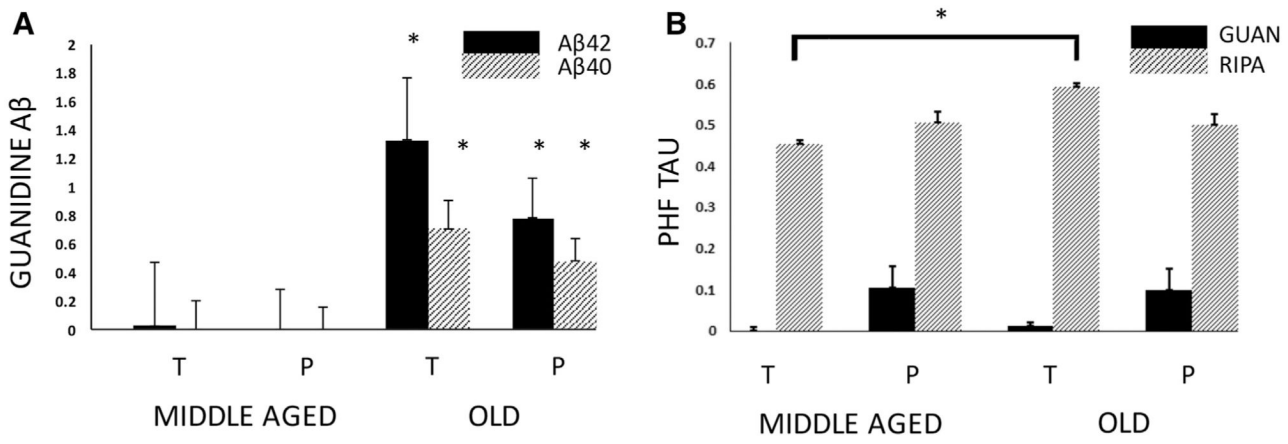

Fig. 4.

(A) Guanidine-extracted $A\beta_{42}$ (dark bars) and $A\beta_{40}$ (striped bars) levels in temporal (T) and parietal (P) cortex (transformed values). Levels were significantly higher in old vervets than middle-aged animals in both regions (all ps < 0.05). (B) Guanidine- (dark bars) and RIPA-extracted (striped bars) PHF tau in temporal (T) and parietal (P) cortex (transformed values). RIPA-extracted PHF-tau was higher in temporal cortex for older animals, whereas no age difference was observed for parietal cortex. Guanidine-extracted levels were significantly higher in parietal than temporal cortex ($P < .05$) for both age groups. Abbreviations: Aβ, β-amyloid; PHF, paired helical filament.

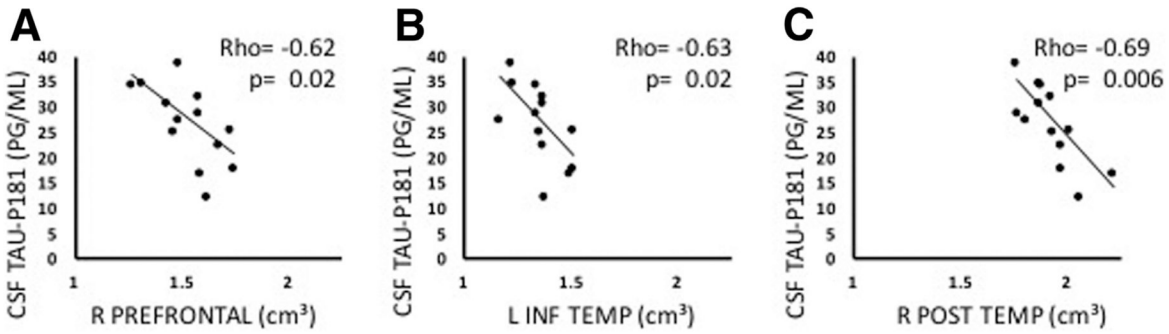

Fig. 5.

Spearman rank-order correlations between CSF tau-P181 and MRI volume for (A) right prefrontal, (B) left inferior temporal, and (C) right posterior temporal regions. Higher tau-p181 values were associated with reduced volumes. Abbreviations: CSF, cerebrospinal fluid; MRI, magnetic resonance imaging.

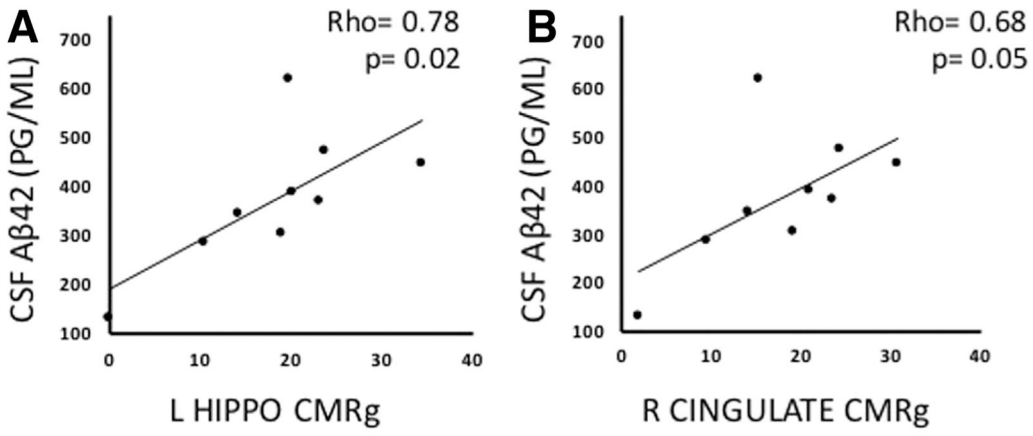

Fig. 6.

Spearman rank order correlations between CSF $A\beta_{42}$ and cerebral metabolic rate of glucose utilization in (A) left hippocampus and (B) right cingulate. Abbreviations: CSF, cerebrospinal fluid; Aβ, β-amyloid.

Table 1

NIA-AA AD Thal phase (A), Braak stage (B), and CERAD (C) scores [20] for middle-aged and old vervets (A, absent = 0; S, sparse = 1; M, moderate = 2; F, frequent = 3)

Group	Age	Thal (A)	Braak (B)	CERAD (C)
Middle-Aged	8.5	0 (0)	0 (0)	A (0)
	8.7	0 (0)	0 (0)	A (0)
	9.8	0 (0)	0 (0)	A (0)
	10.7	0 (0)	0 (0)	A (0)
	10.7	0 (0)	0 (0)	A (0)
	11.5	0 (0)	0 (0)	A (0)
	12.4	1 (1)	0 (0)	S (1)
	12.5	0 (0)	0 (0)	A (0)
	13.7	0 (0)	0 (0)	A (0)
Old	19.7	1 (1)	0 (0)	S (1)
	20.6	1 (1)	0 (0)	A (0)
	21.6	1 (1)	0 (0)	M (2)
	21.6	1 (1)	0 (0)	A (0)
	22.8	2 (1)	0 (0)	F (3)
	23.6	1 (1)	0 (0)	S (1)
	23.6	1 (1)	0 (0)	M (2)
	23.6	1 (1)	0 (0)	F (3)
	23.6	1 (1)	0 (0)	M (2)

Table 2

For amyloid-positive vervets, percent with plaques in individual brain regions (adapted from Thal et al. [24])

Region	Percent with Aβ plaques
Posterior middle temporal gyrus	80%
Posterior cingulate gyrus	70%
Anterior superior temporal gyrus	60%
Anterior middle temporal gyrus	50%
Insular cortex	50%
Posterior precentral gyrus	50%
Occipital gyrus	50%
Anterior cingulate gyrus	50%
Supramarginal gyrus	50%
Postcentral gyrus	50%
Superior frontal gyrus	50%
Fusiform gyrus	40%
Superior parietal lobule	40%
Anterior inferior temporal gyrus	40%
Posterior superior temporal gyrus	30%
Posterior inferior temporal gyrus	30%
Anterior precentral gyrus	30%
Lingual gyrus	30%
Hippocampus	10%
Subiculum	0%
Caudate nucleus	0%
Putamen	0%

Abbreviation: Aβ, β-amyloid.

Table 3

Brain regions with PHF-tau and the frequency of positivity among all vervets, ranked from highest to lowest (adapted from Thal et al. [27])

Region	Percent with PHF-tau
Superior occipital gyrus	89%
Cingulate	78%
Cuneus	72%
Caudate nucleus	67%
Entorhinal cortex	67%
Insular cortex	61%
Putamen	61%
Superior parietal lobule	61%
Precentral gyrus	56%
Fusiform gyrus	56%
Superior frontal gyrus	50%
Middle temporal gyrus	50%
Inferior temporal gyrus	50%
Lingual gyrus	50%
Postcentral gyrus	44%
Superior temporal gyrus	44%
Supramarginal gyrus	39%
Inferior occipital gyrus	39%
Globus pallidus	22%
Subiculum	17%
Hippocampus	17%

Abbreviation: PHF, paired helical filament.